

PSR J1833–1034: DISCOVERY OF THE CENTRAL YOUNG PULSAR IN THE SUPERNOVA REMNANT G21.5–0.9

F. CAMILO,¹ S. M. RANSOM,² B. M. GAENSLER,^{3,4} P. O. SLANE,³ D. R. LORIMER,⁵ J. REYNOLDS,⁶ R. N. MANCHESTER,⁷ AND S. S. MURRAY³

Received 2005 May 22; accepted 2005 September 26

ABSTRACT

We have discovered the pulsar associated with the supernova remnant G21.5–0.9. PSR J1833–1034, with spin period $P = 61.8$ ms and dispersion measure $169 \text{ cm}^{-3} \text{ pc}$, is very faint, with pulse-averaged flux density of $\approx 70 \mu\text{Jy}$ at a frequency of 1.4 GHz, and was first detected in a deep search with the Parkes telescope. Subsequent observations with Parkes and the Green Bank Telescope have confirmed this detection, and yield a period derivative $\dot{P} = 2.02 \times 10^{-13}$. These spin parameters imply a characteristic age $\tau_c = 4.8$ kyr and a spin-down luminosity $\dot{E} = 3.3 \times 10^{37} \text{ ergs s}^{-1}$, the latter value exceeded only by the Crab pulsar among the rotation-powered pulsars known in our Galaxy. The pulsar has an unusually steep radio spectrum in the 0.8–2.0 GHz range, with power law index ≈ 3.0 , and a narrow single-peaked pulse profile with full-width at half maximum of $0.04P$. We have analyzed 350 ks of archival *Chandra X-ray Observatory* High Resolution Camera (HRC) data, and find a point-like source of luminosity $\approx 3 \times 10^{-5} \dot{E}$, offset from the center of an elliptical region of size $\approx 7'' \times 5''$ and luminosity $\approx 10^{-3} \dot{E}$ within which likely lies the pulsar wind termination shock. We have searched for X-ray pulsations in a 30 ks HRC observation without success, deriving a pulsed fraction upper limit for a sinusoidal pulse shape of about 70% of the pulsar flux. We revisit the distance to G21.5–0.9 based on HI and CO observations, arguing that it is 4.7 ± 0.4 kpc. We use existing X-ray and radio observations of the pulsar wind nebula, along with the measured properties of its engine and a recent detection of the supernova remnant shell, to argue that G21.5–0.9 and PSR J1833–1034 are much younger than τ_c , and likely their true age is $\lesssim 1000$ yr. In that case, the initial spin period of the pulsar was $\gtrsim 55$ ms.

Subject headings: ISM: individual (G21.5–0.9) — pulsars: individual (PSR J1833–1034) — supernova remnants — stars: neutron

1. INTRODUCTION

“Crab-like” remnants of supernovae (SNe) display no readily observable manifestation of an ejecta-driven blast wave; instead, the relativistic wind of particles and magnetic fields released by a young pulsar is confined by the ambient pressure giving rise to a non-thermal compact nebula. Such pulsar wind nebulae (PWNe), particularly with knowledge of the spin parameters of their central engines, are magnificent laboratories for the study of astrophysical shocks, the properties of pulsar winds, and the spin evolution and birth parameters of neutron stars. Eventually, depending on explosion energy and environment, high velocity SN ejecta are expected to generate a brightening shell surrounding the PWN, creating a “composite” supernova remnant (SNR).

G21.5–0.9, known for 35 years (Altenhoff et al. 1970; Wilson & Altenhoff 1970) and long-classified (Wilson & Weiler 1976; Becker & Szymkowiak 1981) as one of about ten Crab-like remnants (Green 2004), is a bright and absorbed (neutral hydrogen column density $N_H = 2 \times 10^{22} \text{ cm}^{-2}$; Safi-Harb et al. 2001) centrally peaked X-ray and polarized radio source. HI absorption measure-

ments (Caswell et al. 1975; Davelaar, Smith, & Becker 1986) place the system at > 4.4 kpc. Its radio and X-ray luminosities are ~ 10 and ~ 100 times below those of the Crab Nebula, respectively (Helfand & Becker 1987). A break in the observed spectrum of G21.5–0.9 was originally reported at a frequency $\nu_b \sim 50$ GHz (e.g., Salter et al. 1989), although more recently it has been suggested that $\nu_b \gtrsim 500$ GHz (Gallant & Tuffs 1998; Bock, Wright, & Dickel 2001; Bandiera, Neri, & Cesaroni 2001).

X-ray observations in the modern era have advanced our knowledge of G21.5–0.9 enormously. At the center of the system is a bright compact source ($\approx 2''$ in radius; Slane et al. 2000) that may include the pulsar and delineate its wind termination shock. Surrounding this is the previously known PWN ($\approx 40''$ in radius), which is more compact than the radio nebula, and with a spectrum that steepens radially from the center (e.g., Safi-Harb et al. 2001; Warwick et al. 2001; Bock et al. 2001). But most remarkably, surrounding the PWN is a low surface-brightness non-thermal halo, $\approx 150''$ in radius, with no radio counterpart (Slane et al. 2000), and apparently with a spatially invariant photon index (Matheson & Safi-Harb 2005). The very deep *Chandra* image presented by Matheson & Safi-Harb (2005) beautifully demonstrates evidence for limb brightening in this halo. It now appears likely that a portion of the emission observed in the halo originates in the long sought SNR shell, while it is possible that dust scattering also contributes significantly to the observed emission (Bocchino et al. 2005), especially within about $80''$ of the center. While unusual, such a non-thermal shell is not unprecedented (e.g., Koyama et al. 1995; Slane et al. 1999), and could be due to relativistic electrons accelerated at the SN ejecta–ambient gas shock front. G21.5–

arXiv:astro-ph/0509823v1 27 Sep 2005

¹ Columbia Astrophysics Laboratory, Columbia University, 550 West 120th Street, New York, NY 10027.

² NRAO, 520 Edgemont Road, Charlottesville, VA 22903.

³ Harvard-Smithsonian Center for Astrophysics, 60 Garden Street, Cambridge, MA 02138.

⁴ Alfred P. Sloan Research Fellow.

⁵ University of Manchester, Jodrell Bank Observatory, Macclesfield, Cheshire, SK11 9DL, UK.

⁶ Australia Telescope National Facility, CSIRO, Parkes Observatory, P.O. Box 276, Parkes, NSW 2870, Australia.

⁷ Australia Telescope National Facility, CSIRO, P.O. Box 76, Epping, NSW 1710, Australia.

0.9 has also been detected in hard X-rays by *INTEGRAL*, with a 20–100 keV flux of ~ 3 millicroabs and a flatter spectrum than that of the Crab Nebula (Bird et al. 2004).

Meanwhile, the pulsar powering the PWN at the center of the composite SNR G21.5–0.9 has remained undetected, despite searches in the radio (e.g., Kaspi et al. 1996; Crawford et al. 2002) and X-ray bands (Slane et al. 2000; Safi-Harb et al. 2001; La Palombara & Mereghetti 2002). We have now, in the course of extensive deep radio searches of PWNe (e.g., Camilo et al. 2002a,c), discovered PSR J1833–1034, the central engine of G21.5–0.9, which we report on here. After submitting this paper, we became aware of an independent discovery of this pulsar by Gupta et al. (2005), whose results on the pulsed signal from this source largely agree with ours.

We begin by describing the pulsar search at radio wavelengths (§ 2.1) and its confirmation and follow-up observations (§ 2.2). We then present an X-ray imaging analysis of G21.5–0.9 (§ 2.3) and search for pulsations (§ 2.4). In § 3.1 we obtain the distance to the system, after which we discuss the wind termination shock region, nebular magnetic field (§ 3.2), and age (§ 3.3) of G21.5–0.9. We compare the properties of PSR J1833–1034 and its SNR to those of SNR 3C 58 and its pulsar in § 3.4, and in § 3.5 we remark on the radio spectrum of PSR J1833–1034, putting it in the context of those of other young pulsars. We summarize our work in § 4.

2. OBSERVATIONS AND ANALYSIS

2.1. Radio Pulsar Search

We observed the position R.A. (J2000) $18^{\text{h}}33^{\text{m}}33^{\text{s}}.8$, Decl. (J2000) $-10^{\circ}34'10''$, centered on G21.5–0.9, at the Parkes 64-m radio telescope on 2002 January 6 for a full transit of 8.0 hr with the central beam of the multibeam receiver system (Staveley-Smith et al. 1996). The observation was centered at a frequency of 1374 MHz, with a bandwidth of 288 MHz for each of two polarizations split into 96 contiguous frequency channels. Total-power signals were detected and sampled with 1-bit precision every 0.8 ms, with a total of 36 million time samples for each of 96 frequency channels recorded to magnetic tape for analysis.

We analyzed the data using standard pulsar search techniques (see, e.g., Lorimer & Kramer 2005) implemented in the PRESTO software package (Ransom 2001; Ransom, Eikenberry, & Middleditch 2002a). While the Cordes & Lazio (2002) model for the Galactic distribution of free electrons predicts a dispersion measure (DM) $> 282 \text{ cm}^{-3} \text{ pc}$ for the distance to G21.5–0.9 of $> 4.4 \text{ kpc}$, such predictions can be inaccurate (e.g., Halpern et al. 2001; Camilo et al. 2002d), and we searched the DM range $0\text{--}2674 \text{ cm}^{-3} \text{ pc}$, up to twice the maximum expected Galactic value in this direction. We first analyzed the non-dispersed (i.e., $\text{DM} = 0 \text{ cm}^{-3} \text{ pc}$) data to identify strong interference signals that we subsequently masked (in the time, radio frequency, or fluctuation frequency domains). We de-dispersed, barycentered, and searched the data for each of 524 trial DMs while maintaining close to optimal time resolution throughout the DM range searched. A pulsar with very large spin period derivative, \dot{P} , may change its spin frequency perceptibly within such a long observation, diminishing the sensitivity unless a number of trial acceleration values are used to generate multiple time series to be searched: e.g., the Crab pulsar’s fundamental would move by 0.3 Fourier bins within our observation, and a young pulsar in a binary system could be

TABLE 1
RADIO OBSERVATIONS OF PSR J1833–1034.

Date (MJD)	Telescope	Time (hr)	Frequency (MHz)	Bandwidth (MHz)	Backend ^a	$T_{\text{sys}}^{\text{b}}$ (K)	$S_{\text{PSR}}^{\text{c}}$ (μJy)
52280	Parkes	8.0	1374	288	filter bank	40	66
53474	GBT	0.5	1950	600	SPIGOT	39	...
53479	Parkes	5.9	1374	288	filter bank	40	76
53482	GBT	3.3	820	48	BCPM	83	277
53486	GBT	4.5	1950	600	SPIGOT	39	13
53502	GBT	0.4	820	48	BCPM	83	283
53525	GBT	1.0	820	48	BCPM	83	181
53557	GBT	0.8	820	48	BCPM	83	193
53575	GBT	2.8	820	48	BCPM	83	171

^aFor details on observing equipment, see: filter bank (Manchester et al. 2001); SPIGOT (Ransom et al. 2005; Kaplan et al. 2005); BCPM (Backer et al. 1997; Camilo et al. 2002d).

^bIncludes contribution from Galaxy (scaled from the 408 MHz map of Haslam et al. 1982, with spectral index of 2.6) and SNR ($\approx 6 \text{ Jy}$ at 1 GHz with flat spectrum; Salter et al. 1989).

^cIntegrated period-averaged pulse profile, compared to the rms of the off-pulse region, scaled via the radiometer equation using the observation bandwidth and time, and assuming the nominal telescope gain and system temperature (previous column). For SPIGOT, we used only 1650–2050 MHz data to calculate flux density (see caption to Fig. 1). These estimates have an uncertainty of about 25%, exclusive of variations due to interstellar scintillation.

affected even more by orbital Doppler accelerations. For this reason we used Fourier-domain acceleration searches to cover a range of \dot{P} that would cause a signal to drift by up to ± 16 Fourier bins for the highest of 1, 2, 4, 8, and 16 harmonics. We summed these harmonics incoherently to retain sensitivity to narrow pulse profiles.

We detected a clear pulsar signal at $\text{DM} \approx 170 \text{ cm}^{-3} \text{ pc}$ with barycentric period $P = 61.84 \text{ ms}$, $\dot{P} < 5 \times 10^{-13}$ and a narrow profile with full-width at half maximum of $0.05P$ (Fig. 1, middle panel).

2.2. Confirmation and Follow-up Observations

On 2005 April 14 we observed the pulsar with the 100-m Green Bank Telescope (GBT) for 0.5 hr at a central frequency of 1950 MHz. While the pulsar was not detected in an unbiased way in this short observation, searching a range of periods for assumed values of $\dot{P} \lesssim 5 \times 10^{-13}$ yielded the most promising candidate for $\dot{P} \sim 2 \times 10^{-13}$. On 2005 April 19, we clearly re-detected the pulsar at 1374 MHz at Parkes with $P = 61.86 \text{ ms}$, implying $\dot{P} = 2.02 \times 10^{-13}$. The retrospective detection at GBT also implies that its positional uncertainty from radio observations is about $\pm 3'$ (telescope beamwidth).

We have now observed the new pulsar at 820 MHz, in addition to the two frequencies described above (see Table 1). There is some evidence for fluctuation in received flux density, likely due to interstellar scintillation (see Fig. 1). The flux densities listed in Table 1 are calibrated only approximately, and are therefore subject to some future adjustment. Nevertheless, we infer that the spectrum of the pulsar is steep, with a weighted fit to the values presented in Table 1 giving $\alpha = 3.0 \pm 0.3$ (throughout this paper, $S_{\nu} \propto \nu^{-\alpha}$). The flux density of $\approx 0.65 \text{ mJy}$ at a frequency of 610 MHz estimated by Gupta et al. (2005) is consistent with this determination of α .

The new pulsar has a magnetic field strength at its light cylinder of $B_{\text{lc}} = 1.4 \times 10^5 \text{ G}$, the sixth highest value among pulsars known in the Galactic disk, ex aequo with PSR J2229+6114 (Halpern et al. 2001). Since the emission of “giant” radio pulses appears to be correlated with B_{lc} (e.g.,

TABLE 2
MEASURED AND DERIVED PARAMETERS FOR PSR J1833–1034.

Parameter	Value
Right ascension, R.A. (J2000).....	18 ^h 33 ^m 33 ^s .57
Declination, Decl. (J2000).....	−10°34′07″.5
Spin period, P (s).....	0.061865672117(5)
Epoch (MJD).....	53545.0
Period derivative, \dot{P} ^a	$2.02025(3) \times 10^{-13}$
Period derivative, \dot{P} ^b	$(2.0206 \pm 0.0004) \times 10^{-13}$
Dispersion measure, DM (cm ^{−3} pc).....	169.5(1)
Post-fit rms timing residuals (ms).....	0.23
Data span (MJD).....	53479–53575
Pulse full-width at half-maximum (ms).....	≈ 2.5
Flux density at 820 MHz (μ Jy).....	≈ 221
Flux density at 1374 MHz, S_{1400} (μ Jy).....	≈ 71
Flux density at 1850 MHz (μ Jy).....	≈ 13
Spin-down luminosity, \dot{E} (ergs s ^{−1}).....	3.37×10^{37}
Surface dipole magnetic field strength (gauss) ^c	3.58×10^{12}
Characteristic age, τ_c (kyr).....	4.85
Distance, d (kpc).....	4.7 ± 0.4
Radio luminosity at 1.4 GHz, $S_{1400}d^2$ (mJy kpc ²).....	≈ 1.5
Radio spectral index, α	≈ 3.0

NOTE. — Celestial coordinates are assumed to correspond to the central peak of the X-ray PWN seen in *Chandra* HRC observations (§ 2.3; Fig. 3). Numbers in parentheses are three times the nominal 1σ TEMPO uncertainties in the least-significant digits quoted.

^aThis \dot{P} was determined from the timing solution based on data collected during the span listed.

^bThis \dot{P} was obtained from the TEMPO-derived P for MJD 53545.0 and the period measured from the discovery observation on MJD 52280.

^c $B_p \equiv 3.2 \times 10^{19} (P\dot{P})^{1/2}$ G (see, e.g., Manchester & Taylor 1977).

Cognard et al. 1996; Johnston & Romani 2003), we made a preliminary search for such pulses in the long 820 MHz data set (Table 1), but have not detected any.

We measured pulse times-of-arrival (TOAs) from the GBT and Parkes data and fitted a simple spin-down model to the 2005 TOAs using TEMPO⁸. The results of the fit are shown in Table 2. The position used for the pulsar was that determined from *Chandra* observations (§ 2.3). The \dot{P} measured from the phase-coherent solution at the present epoch matches that derived from two period measurements separated by 3.5 yr.

2.3. X-ray Imaging of G21.5–0.9

G21.5–0.9 is used as a calibration target for the *Chandra* X-ray Observatory, and multiple observations exist using a variety of detector modes and aimpoint positions. For a set of six observations carried out with the Advanced CCD Imaging Spectrometer (ACIS), with the target placed within $1'$ of the optical axis of the telescope and falling on CCD S3, we used the CIAO⁹ task *merge_all* to generate a combined image of the PWN (Fig. 2). The integrated exposure for the image is 58 ks, and we have applied a Gaussian smoothing of two pixels ($0''.98$). The image shows an extended core, identified in earlier *Chandra* observations (Slane et al. 2000; Safi-Harb et al. 2001), surrounded by a broader nebula with a radius of $\approx 40''$. There is considerable structure in the outer nebula region, including filamentary features and a distinct low-surface-brightness “notch” in the outer northwest of the PWN (see also Safi-Harb et al. 2001; Matheson & Safi-Harb 2005). We split the image in Figure 2 into two energy bands (0.3–6.0 keV and 6.0–10.0 keV) and computed radial surface

brightness profiles: the profile in the hard band is slightly steeper than that in the soft band, although X-ray emission extends in both bands to roughly the same outer radius.

To further investigate the compact core, we created a merged image from 21 observations with the *Chandra* High Resolution Camera (HRC), using data from both the imaging (HRC-I) and spectroscopy (HRC-S) cameras (the latter used here without transmission gratings). The emission-line star SS 397 was identified in the field of each observation, and its 2MASS position (R.A. [J2000] 18^h33^m27^s.70, Decl. [J2000] −10°35′23″.0) was used to register separately each individual observation in order to improve the overall astrometry. The resulting merged image of the core region, corresponding to a total integration of 351 ks, is shown in Figure 3. With a typical 2MASS positional uncertainty of $\lesssim 0''.2$ and determination of the X-ray centroid to better than an HRC pixel, we estimate that any residual blurring/registration error in this image is at the level of $< 0''.3$. A comparison of Figure 3 with Figure 4 of Safi-Harb et al. (2001) reveals significant differences in morphology, plus an offset of $\sim 1''.5$ in the position of peak emission. Safi-Harb et al. (2001) did not discuss any efforts to correctly register each exposure, and it is possible that their image has been affected by slight shifts between observations.

Immediately evident in Figure 3 is a compact source surrounded by an elliptical emission region of size $\approx 7'' \times 5''$ (in a very saturated image, this core appears to be about 50% larger in each dimension; see, e.g., Fig. 2). This is to be compared with the 90% encircled-energy radius of $\approx 1''$ for HRC. The point-like source is located at R.A. (J2000) 18^h33^m33^s.57, Decl. (J2000) −10°34′07″.5 and offset from the center of the ellipse, possibly indicating a Doppler-boosted toroidal structure surrounding a pulsar, as is observed for the Crab and other pulsars imaged with *Chandra* (e.g., Ng & Romani 2004; Hessels et al. 2004; Slane et al. 2004). In this scenario, the inferred pulsar spin axis projected on the sky is perpendicular to the major axis of the ellipse, at a position angle of $\sim 40^\circ$ north through east (similar to the position angle first suggested by Fürst et al. 1988, for the central source in G21.5–0.9). The major axis of the ellipse is aligned toward the notch of reduced emission on the northwest rim of the PWN (Fig. 2; see also Matheson & Safi-Harb 2005). We note the similarity with the “bays” observed in the Crab Nebula, which are roughly aligned with the torus surrounding its pulsar (e.g., Fesen, Martin, & Shull 1992).

In order to estimate the flux of what is presumed to be the pulsar, we used the CIAO package Sherpa to perform spatial modeling in which we fit the core region of G21.5–0.9 (Fig. 3) to a model consisting of a point source (convolved with the PSF, calculated using the CIAO task *mkpsf* for an energy of 1 keV), a 2-D Gaussian, and a constant background. While the extended emission is clearly not a 2-D Gaussian (we expect perhaps a Doppler-brightened torus superimposed on more uniform emission), this is the most suitable model available in Sherpa and provides a good fit. As expected, the best-fit values for the point-source position and Gaussian centroid are very different, limiting the point source flux assigned to the Gaussian component. In any case, there is a systematic uncertainty in this flux determination in excess of the formal fit uncertainty of 10%, and a more realistic geometrical modeling is required to improve significantly on this result. In the energy range 0.5–10 keV, the resulting count rate for the pulsar is $1.5 \times 10^{-3} \text{ s}^{-1}$, corresponding to an unabsorbed flux of about $2.8 \times 10^{-13} \text{ ergs cm}^{-2} \text{ s}^{-1}$ for a spectral index of $\alpha_X = 0.5$, assuming $N_H = 2.2 \times 10^{22} \text{ cm}^{-2}$ (Safi-Harb et al. 2001), or a lu-

⁸ See <http://pulsar.princeton.edu/tempo>.

⁹ See <http://cxc.harvard.edu/ciao>.

minosity of about 9×10^{32} ergs s^{-1} at a distance of 5 kpc (see § 3.1). The assumed N_H may be somewhat in error, since simple fits to the data yield values of N_H that differ by as much as 20% depending on radial position within the nebula. However, such a variance in N_H introduces a variation of only 20% on the point source flux, smaller than the uncertainty arising from the difficulties involved in spatial modeling. Through such an absorbing column and at a distance of 5 kpc, thermal radiation from a 10 km-radius neutron star with a surface temperature of 1.4 MK (appropriate for standard cooling to an age ~ 1000 yr; see § 3.3) would contribute an HRC count rate of only $\sim 10\%$ that observed, and we do not consider it further here.

The entire elliptical region of X-ray emission shown in Figure 3, including the compact component, has a 0.5–10 keV count rate of $6.1 \times 10^{-2} s^{-1}$. Assuming $\alpha_X = 1.0$ and $N_H = 2.2 \times 10^{22} cm^{-2}$, this corresponds to an unabsorbed 0.5–10 keV flux of 1×10^{-11} ergs $cm^{-2} s^{-1}$ or a luminosity at 5 kpc of 3×10^{34} ergs s^{-1} .

2.4. Search for X-ray Pulsations

G21.5–0.9 was observed for 30 ks with the *Chandra* HRC-S on 2002 November 12 (ObsID 2755), with the detector operated in timing mode. In this mode, event arrival times are adjusted to compensate for a wiring error, allowing photons to be time-tagged to a resolution of $16 \mu s$. We corrected these event times to the Solar System barycenter using the CIAO task *axbary* and the nominal pulsar position (§ 2.3). We extracted 558 events from a circular region of radius $1''$, centered on the position of the compact source identified in the merged HRC image (Fig. 3). We searched these events for pulsations around the spin frequency predicted by the radio ephemeris (Table 2), covering approximately 3 independent Fourier spacings (10^{-4} Hz). We used the Discrete Fourier Transform, which is optimally sensitive to sinusoidal pulsations, and the Bayesian technique of Gregory & Loredo (1992), which is sensitive to pulsations with a more complex but unknown shape. In neither case did we find any evidence of X-ray pulsations. We estimate a 99% confidence-level upper limit on the pulsed fraction for sinusoidal pulsations of 21%, using the method described by Ransom, Gaensler, & Slane (2002b). If the pulsar has a significantly narrower X-ray pulse profile, as in the radio, the pulsed fraction would be significantly less than 21% (with the exact value depending sensitively on the pulse shape). This limit pertains to pulsations from the total observed flux within the extraction region and does not apply to the pulsar’s flux alone. Since the pulsar likely contributes $\lesssim 30\%$ of the counts in the region considered, our upper limit represents a significant fraction ($\sim 70\%$) of the total signal from the pulsar, and hence is not especially constraining.

3. DISCUSSION

The P and \dot{P} of the newly discovered pulsar imply a characteristic age $\tau_c \equiv P/(2\dot{P}) = 4.8$ kyr and spin-down luminosity $\dot{E} \equiv 4\pi^2 I \dot{P} P^{-3} = 3.3 \times 10^{37}$ ergs s^{-1} , where the neutron star moment of inertia is $I \equiv 10^{45}$ g cm^2 . This \dot{E} is remarkably similar to that predicted by Slane et al. (2000) for the pulsar in G21.5–0.9 based on the X-ray energetics of the PWN, and is second only to that of the Crab among known Galactic rotation-powered pulsars. Still, until X-ray pulsations are detected from the core of the PWN with $P = 61.8$ ms or until the positional uncertainty of the pulsar is reduced to a few

arcsec, it could be argued that it may not be the counterpart of the PWN. However, if the newly discovered pulsar were not associated with G21.5–0.9, we would certainly expect to detect it in the deep *Chandra* observations of the field, given its relatively small inferred distance (§ 3.1) and large \dot{E} , and no such potential counterpart exists (e.g., Matheson & Safi-Harb 2005). Therefore, this is clearly the neutron star responsible for the PWN in G21.5–0.9, which we designate PSR J1833–1034 based on the position of the central compact source detected with *Chandra* (Fig. 3; see also § 2.3 and Table 2).

3.1. Distance to G21.5–0.9 and PSR J1833–1034

To derive an upper limit on the distance to G21.5–0.9, we consider the bright extragalactic source PMN J1832–1035, which lies just $18'$ from G21.5–0.9. An H I absorption spectrum of PMN J1832–1035, using data taken from the Very Large Array Galactic Plane Survey (Taylor et al. 2002), shows a strong absorption feature at a local standard of rest (LSR) velocity of $+76$ km s^{-1} , but which is not seen toward G21.5–0.9 (Caswell et al. 1975; Davelaar et al. 1986). The CO survey of Dame, Hartmann, & Thaddeus (2001) shows a bright coherent region of molecular material at this velocity, present in the direction of both PMN J1832–1035 and G21.5–0.9. Thus, it is highly likely that there is cold neutral gas at an LSR velocity of $+76$ km s^{-1} toward both sources. The lack of H I absorption against G21.5–0.9 at this velocity implies that the SNR is in front of this cloud.

We next compare the emission spectrum of this CO to the H I emission survey of Hartmann & Burton (1997). In the direction of PMN J1832–1035, the H I emission shows a narrow feature of reduced emission in the spectrum at a velocity of $+76$ km s^{-1} . We interpret this feature as H I self-absorption, indicating that cold gas on the near side of the tangent point is absorbing H I emission produced on the far side (Liszt, Burton, & Bania 1981; Jackson et al. 2002). Using the Galactic rotation curve of Fich, Blitz, & Stark (1989) and assuming a Galactocentric radius for the Sun of 8.5 kpc, the distance to this cloud and hence an upper limit on the distance to G21.5–0.9 is 4.9 kpc. Combined with previous H I measurements that put a lower limit on the SNR’s systemic LSR velocity of 65 km s^{-1} (Davelaar et al. 1986), corresponding to a distance limit of 4.4 kpc, and adopting an uncertainty in the systemic velocity of H I clouds of ± 7 km s^{-1} (Shaver et al. 1982; Belfort & Crovisier 1984), we conclude that the kinematic distance to SNR G21.5–0.9 is 4.7 ± 0.4 kpc.

The Cordes & Lazio (2002) model yields a distance $d = 3.3$ kpc for PSR J1833–1034, which is clearly an underestimation of the true distance, but supports a relatively small value. Safi-Harb et al. (2001) have estimated $4.1 < d < 5.2$ kpc from a calibration to a range of X-ray-derived N_H values. Hereafter we scale the distance to PSR J1833–1034 and G21.5–0.9 in terms of $d_5 \equiv d/(5 \text{ kpc})$.

The X-ray spectra of the various components of G21.5–0.9 imply a foreground absorbing column $N_H \approx 2 \times 10^{22} cm^{-2}$ (Warwick et al. 2001; Safi-Harb et al. 2001). Comparison with the DM given in Table 2 implies a ratio $N_H/DM \approx 40$. This is substantially higher than seen toward all but ~ 3 other pulsars (see discussion in Gaensler et al. 2004). Gaensler et al. argue that these high ratios indicate that a source is behind a substantial amount of molecular material. Indeed, the CO data of Dame et al. (2001) indicate at least three CO clouds at LSR velocities between 0 and 75 km s^{-1} , which presumably contribute to the high observed neutral column.

3.2. Relativistic Wind Termination Shock and Nebular Magnetic Field

Knowing \dot{E} for PSR J1833–1034, we can estimate the termination shock radius, r_s , at which the pulsar wind pressure, $\dot{E}/(4\pi r_s^2 \eta c)$, balances the interior pressure of the nebula, P_n , where η is the fractional solid angle covered by the pulsar wind. Assuming nebular equipartition between particles and fields, $P_n = B_n^2/(4\pi)$, and we have $\theta_s = 0''.46 \eta^{-1/2} d_5^{-1} B_{\text{mG}}^{-1}$, where B_{mG} is the nebular field in mG and $\theta_s = r_s/d$. The field derived from equipartition arguments (e.g., Pacholczyk 1970) for the whole PWN is $B_n \approx 0.3$ mG (where we have used a spectral index of $\alpha_r = 0$ between 100 MHz and 500 GHz; see Bandiera et al. 2001, and references therein), implying $\theta_s \approx 1''.6 \eta^{-1/2}$. This can be compared with Figure 3, from which we infer that $\theta_s \lesssim 2''.5$ (note however that we do not actually observe a limb-brightened ring-like structure, as is the case in some PWNe, and it is presumably also possible that $\theta_s \lesssim 1''$). The approximate match between estimated and inferred shock radii suggests that the nebular magnetic field strength is indeed relatively large, as estimated from equipartition arguments.

For such a relatively high field, the synchrotron lifetime of relativistic electrons that emit 2 keV photons is only ~ 20 yr. Assuming a nebular flow velocity profile of $V(r) = (c/3)(r_s/r)^2$ (Kennel & Coroniti 1984), these electrons would travel $\sim 12''$ before radiative losses become important. (The equivalent nebular flow timescale to the edge of the PWN is $\gtrsim 500$ yr.) According to Matheson & Safi-Harb (2005), the X-ray spectrum steepens significantly beyond its slope close to the pulsar at a radius $\gtrsim 10''$ – $15''$ (which also appears to be the approximate angular scale of the relatively bright X-ray “plateau” seen in Fig. 2). Additionally, it appears that the normalized X-ray and radio surface brightness profiles begin to diverge, with the nebula becoming effectively smaller at X-ray energies, at $\gtrsim 10''$ (Bock et al. 2001; Dickel & Wang 2004, see also § 2.3). Overall, it thus appears that a relatively high nebular field strength is compatible with many of the observations.

A break in the spectrum of G21.5–0.9 is inferred at $\nu_b \gtrsim 500$ GHz ($\lambda_b \lesssim 1$ mm; Gallant & Tuffs 1998; Bock et al. 2001; Bandiera et al. 2001). However, for an age $\gtrsim 500$ yr and $B_n \approx 0.25$ mG, one expects a break in the spectrum due to synchrotron cooling at $\lesssim 1$ μm . The sub-millimeter break must then be due to something else, presumably reflecting the complex nature (or variability) of the spectrum injected by the pulsar or of its conversion to detectable electromagnetic radiation.

3.3. The Evolutionary State and Age of G21.5–0.9

For spin evolution with constant magnetic moment, the age of a pulsar is $\tau = PP^{-1}(n-1)^{-1}[1 - (P_0/P)^{n-1}]$; the index n is 3 for dipole braking (in the few cases measured, $1.5 \lesssim n \lesssim 3$; e.g., Camilo et al. 2000, and references therein). Further assuming that the initial spin period $P_0 \ll P$, reduces the age to τ_c , or 4.8 kyr in the case of PSR J1833–1034. Hereafter we scale the age of the pulsar/SNR system by $\tau_5 \equiv \tau/(5 \text{ kyr})$, and now show from multiple lines of evidence that in fact $\tau_5 \ll 1$.

The scale of structures in G21.5–0.9 is $R = 1 d_5 \theta_{40}$ pc, where we scale angular sizes by $\theta_{40} \equiv \theta/(40'')$. Corresponding velocities are $V = 200 d_5 \tau_5^{-1} \Delta \theta_{40} \text{ km s}^{-1}$, where $\Delta \theta_{40}$ is a change of angular position in units of $40''$. For the PWN, $\theta_{40} \approx 1$, and for the SNR shell, $\theta_{40} \approx 150/40$; thus, $R_{\text{PWN}} \approx 1 d_5$ pc and $R_{\text{SNR}} \approx 3.6 d_5$ pc. Both of these are small, similar to the

corresponding sizes in G11.2–0.3, a 1600 year-old composite SNR (Kaspi et al. 2001; Chevalier 2005).

PSR J1833–1034 is located very near the geometrical center of the G21.5–0.9 shell. Using the image presented by Matheson & Safi-Harb (2005), we estimate that the pulsar’s offset from the center is $\Delta \theta \lesssim 5''$. If the center corresponds to the SN site, the implied projected space velocity is $V_{\text{PSR}} \lesssim 25 d_5 \tau_5^{-1} \text{ km s}^{-1}$. Unless $\tau_5 \ll 1$, this is a very small velocity for a young pulsar (e.g., Lyne & Lorimer 1994; Hobbs et al. 2005, according to whom the probability of $V_{\text{PSR}} < 25 \text{ km s}^{-1}$ is 0.45%). This reasoning was used also by Kaspi et al. (2001) to argue that $\tau \ll \tau_c$ for the pulsar in G11.2–0.3.

The shell in G21.5–0.9 is very faint in X-rays (Matheson & Safi-Harb 2005) and has not yet been detected at radio wavelengths (Slane et al. 2000). This suggests that the system is only slightly more evolved than the Crab, i.e., the shell is only now becoming visible and the SNR is on its way to becoming a clear-cut composite like G11.2–0.3 (in detail, such an argument requires of course an understanding of the circumstellar environments and explosion dynamics). In any case, for a uniform hydrogen ambient medium of density $n_0 \text{ cm}^{-3}$, the SNR has swept up only $M_{\text{sw}} \sim 5 n_0 d_5^3 M_\odot$ and thus should be in nearly free expansion. For an ejected mass of $M_{\text{ej}} = 10 M_{10} M_\odot$ and SN explosion kinetic energy of $10^{51} E_{51} \text{ ergs}$, the expansion velocity would be $3200 (E_{51}/M_{10})^{1/2} \text{ km s}^{-1}$, implying $\tau_5 = 0.25 d_5 (M_{10}/E_{51})^{1/2}$. Since a freely expanding SNR would in reality have a steep density profile to its ejecta, these estimates of expansion velocity and age are likely to be lower and upper limits, respectively.

Alternatively, let us consider that the expansion has entered the adiabatic phase. Using the Sedov solution, $R_{\text{SNR}} = 0.31 (E_{51}/n_0)^{1/5} t_{\text{yr}}^{2/5} \text{ pc}$. If $\tau_5 = 1$, then $n_0/E_{51} = 120 d_5^{-5}$. Such a high ambient density is clearly inconsistent with the low levels of observed X-ray emission. If conversely we adopt typical values of $n_0/E_{51} \lesssim 1$, then $\tau_5 \lesssim 0.1 d_5^{5/2}$. But in this case the argument is not self-consistent, because then we would have $M_{\text{sw}} < M_{\text{ej}}$. The SNR is therefore still in nearly free expansion, for which the arguments in the above paragraph apply¹⁰.

Consideration of PWN evolution arguments also suggests $\tau_5 \ll 1$. In general, the ratio $R_{\text{PWN}}/R_{\text{SNR}}$ is initially small as the freely expanding ejecta move faster than the PWN expansion rate of $\sim 1000 \text{ km s}^{-1}$. However, the PWN expansion accelerates with the energy input by the pulsar and this ratio increases quickly. After the SNR ejecta decelerate and the reverse shock begins to compress the PWN, the ratio decreases. Since the PWN in G21.5–0.9 is approximately circular, is symmetrically placed within the SNR shell, and has the pulsar at its center, it is likely to be in its early pre-reverse-shock evolutionary stage. For the observed ratio $R_{\text{PWN}}/R_{\text{SNR}} \approx 0.25$, the models of Blondin, Chevalier, & Frierson (2001) are indicative of a very small age. Alternatively, considering simply a constant PWN expansion velocity of $1000 V_{1000} \text{ km s}^{-1}$ (for comparison, the Crab Nebula is expanding at $\sim 1500 \text{ km s}^{-1}$; Bietenholz et al. 1991, and references therein), the observed PWN size implies $\tau_5 = 0.2 d_5 V_{1000}^{-1}$.

The PWN energetics also provide useful insight into the

¹⁰ If $M_{\text{ej}} \ll 10 M_\odot$, as can occur, for instance, in type Ib/Ic SNe, then it does not follow directly from these simple arguments that $M_{\text{sw}} < M_{\text{ej}}$. However, in a detailed spectroscopic and spatial analysis of X-ray data on G21.5–0.9, Bocchino et al. (2005) suggest that $M_{\text{sw}} \lesssim 0.5 M_\odot$, and that in fact the remnant has not yet entered the adiabatic phase.

age of G21.5–0.9. According to Chevalier (2005), the ratio $E_{\text{int}}/(\dot{E}\tau)$ separates “young” (ratio < 1) from older PWNe, where E_{int} is the internal energy of the PWN. A lower limit on E_{int} can be calculated from synchrotron emission, equivalent to approximate equipartition between particles and fields, which is roughly consistent with observations of PWNe. We use equation (46) of Chevalier (2005) to calculate that for G21.5–0.9, $E_{\text{min}} \sim 2.9 \times 10^{47} d_5^{17/7}$ ergs. Here we have used $p_1 = 1 + 2\alpha_r \approx 1.04$ (Salter et al. 1989) and $p_2 = 1 + 2\alpha_X \approx 3$ (Safi-Harb et al. 2001), as well as $\nu_b = 500$ GHz and $L_{\nu b} \approx 1.2 \times 10^{23} d_5^2 \text{ ergs s}^{-1} \text{ Hz}^{-1}$, where p_1 and p_2 are the energy indices for radio- and X-ray-generating particles, respectively, and $L_{\nu b}$ is the spectral luminosity at ν_b . With the measured \dot{E} for PSR J1833–1034, we have $\dot{E}\tau = 5.3 \times 10^{48} \tau_5$ ergs, which is larger than E_{int} (typically within a factor of a few of E_{min}) for any reasonable age. This then implies $\tau \ll \tau_c$ (see Chevalier 2005).

These various arguments all lead to the conclusion that for PSR J1833–1034 and G21.5–0.9, $\tau_5 \ll 1$, and maybe $\tau \lesssim 1000$ yr (a similar conclusion was reached independently by Bocchino et al. 2005, who in an analysis of X-ray data on G21.5–0.9 obtain an age range of 200–1000 yr). In turn this suggests that $P_0 \gtrsim 55$ ms essentially independent of braking index. Measuring n would of course be very interesting and would further constrain the rotational history of J1833–1034, but this is often impossible. For example, for PSR J0205+6449 in SNR 3C 58, the rotational instability of the neutron star prevents n from being determined (Ransom et al. 2004).

While the age inferred here would make PSR J1833–1034 among the 2–3 youngest known neutron stars in the Galaxy, it is highly unlikely that its progenitor SN was observed as an historical event (and indeed no SN is recorded in this direction in the compilation of Stephenson & Green 2002). The observed hydrogen column density corresponds to a visual extinction of 10–11 magnitudes. The peak visual magnitude of the supernova might thus have been only 5–6 (for an absolute magnitude $M_V = -18.5$), which is likely to have gone unnoticed.

3.4. Comparison of G21.5–0.9, 3C 58 and their Pulsars

The measured spin parameters of PSR J1833–1034 are very similar to those of PSR J0205+6449 (Murray et al. 2002), the central engine in 3C 58 (another famous SNR long-classified as Crab-like, from which faint thermal emission has now been detected; see Bocchino et al. 2001; Slane et al. 2004). It is therefore of interest to compare the properties of the respective PWNe, and we list some important parameters of both systems in Table 3.

Most noticeably, 3C 58 is a much larger and more asymmetric PWN than G21.5–0.9, and its ratio of X-ray luminosity to spin-down luminosity, L_X/\dot{E} , is ≈ 11 times smaller. The inferred pulsar wind shock radii differ by a factor of $\gtrsim 3$, but this is understandable if the nebular pressures differ by an order of magnitude, which may well be the case, as inferred from the respective equipartition field estimates (see also § 3.2). Also, the break frequency ν_b for 3C 58 seems to be ~ 10 times lower than for G21.5–0.9¹¹.

¹¹ This may or may not be of significance. Spectral indices have not been reliably measured just below and above the putative ν_b for either of these systems, and a “break” frequency is instead inferred from extrapolations of fluxes measured 1–2 orders of magnitude apart. The complexity of the broad band emission from these PWNe may not be encapsulated by references to,

TABLE 3
PARAMETERS OF PWN G21.5–0.9, 3C 58, AND THEIR PULSARS.

Parameter	G21.5–0.9	3C 58
Distance, d (kpc)	4.7	3.2
PWN size (pc ²) ^a	1.8×1.8	10×5
Termination shock radius, r_s (pc)	$\lesssim 0.05$	≈ 0.15
Radio luminosity (10^7 – 10^{11} Hz), (10^{34} ergs s ^{−1})	1.4	3.0
Radio spectral index, α_r	0.0	0.1
Break frequency, ν_b (GHz)	$\gtrsim 500?$	~ 50
Minimum internal energy, E_{min} (ergs)	$\sim 2.5 \times 10^{47}$	$\sim 10^{48}$
X-ray luminosity (0.5–10 keV), L_X (10^{35} ergs s ^{−1})	2.8	0.2
X-ray spectral index, α_X ^b	0.4–1.3	0.6–1.6
Equipartition magnetic field strength, B_r (mG)	≈ 0.3	≈ 0.08
Age, τ (kyr)	$\lesssim 1000?$	824?
Pulsar period, P (ms)	61.8	65.6
Spin-down luminosity, \dot{E} (10^{37} ergs s ^{−1})	3.3	2.7
Characteristic age, τ_c (kyr)	4.8	5.4
Initial spin period, P_0 (ms)	$\gtrsim 55?$	$\sim 60?$

NOTE. — We use the nominal distances listed here to infer all quantities that depend thereon. Parameters for G21.5–0.9 are from this work and its references, while those for 3C 58 are from Slane et al. (2004) and references therein.

^aAt least in projection, G21.5–0.9 is approximately round (Fig. 2) and 3C 58 is elongated. In both PWNe, the X-ray nebula is somewhat smaller than the radio nebula, an effect more pronounced in G21.5–0.9 (Bock et al. 2001).

^bBoth X-ray spectra steepen radially from the center in similar fashion, within the ranges of α_X indicated (Safi-Harb et al. 2001; Slane et al. 2004; Matheson & Safi-Harb 2005).

3C 58 is widely thought to be the remnant of SN 1181 CE (Stephenson & Green 2002). In order to bring the historical age and measured spin parameters into agreement, Murray et al. (2002) proposed that the initial period of the pulsar was $P_0 \sim 60$ ms, comparable to what we infer for PSR J1833–1034 (§ 3.3). On the other hand, good arguments suggest that 3C 58 may be older (Bietenholz, Kassim, & Weiler 2001), in which case $P_0 \ll 60$ ms. In any case, different spin histories cannot explain different present-day values of L_X , since the relevant electrons/positrons cool relatively quickly in both PWNe.

If its apparently lower inferred ν_b and steeper X-ray spectrum are of significance, much of the pulsar power in 3C 58 may be deposited at lower particle energies, and hence radiated at lower frequencies, compared to the case for G21.5–0.9. In addition, the lower nebular magnetic field strength inferred for 3C 58 (see Table 3) means that its relativistic particles are relatively poor radiators, and this may explain the vastly different X-ray efficiencies in the two systems.

But why is the nebular field strength in 3C 58 apparently so much lower than for G21.5–0.9? If 3C 58 is not the remnant of SN 1181 CE but is substantially older, as argued by Bietenholz et al. (2001) and Chevalier (2005), then the larger PWN size would follow naturally, and its field would also have decayed. Alternatively, even if the ages for both systems are similar, the PWN radius at early stages depends on SN and pulsar properties as $R \propto \dot{E}^{1/5} E_{\text{SN}}^{3/10} M_{\text{ej}}^{-1/2}$, where E_{SN} and M_{ej} are the kinetic energy and ejected mass, respectively, of the associated supernova explosion (Reynolds & Chevalier 1984; van der Swaluw et al. 2001). Therefore, it may be possible to obtain a larger size and lower magnetic field for 3C 58 if either the supernova explosion was more energetic or the ejected mass smaller than the case for G21.5–0.9, either of which are reasonable. Additionally, perhaps insta-

e.g., a single value of ν_b .

bilities in the magnetic field downstream of the termination shock are also of relevance for explaining the elongated shape of 3C 58 and maybe its size (see, e.g., van der Swaluw 2003; Slane et al. 2004).

Finally, we note that the order of magnitude discrepancy in L_X/\dot{E} between PSRs J1833–1034 and J0205+6449, two pulsars with near-identical spin parameters, makes it clear that the predictive power of simple relations between \dot{E} and L_X for pulsars and their PWNe (Seward & Wang 1988; Becker & Trümper 1997; Possenti et al. 2002) is limited.

3.5. The Radio Spectrum of PSR J1833–1034 and Young Pulsars

The radio spectrum of PSR J1833–1034 between 0.8 GHz and 2.0 GHz is unusually steep ($\alpha \approx 3.0$; see § 2.2). Lorimer et al. (1995) show that the mean spectral index for pulsars is ≈ 1.6 , with a suggestion that it is smaller (~ 1) for young pulsars. The Crab pulsar is an exception, with $\alpha = 3.1$. PSR J1833–1034 has a pulse duty cycle of 4%, smaller than virtually all pulsars with $P < 0.1$ s (but similar to that of J0205+6449 in 3C 58, which has similar period as well, and $\alpha \sim 2$; Camilo et al. 2002d). With such a steep spectrum, the pulsar is easier to detect at low frequencies, such as 820 MHz at GBT. However, for good reasons, the first frequency of choice to employ in searching for distant pulsars along the Galactic plane remains 1400 MHz. At this frequency, PSR J1833–1034 has a very low flux density and its luminosity $L_{1400} \equiv S_{1400}d^2 \approx 1.8d_5^2$ mJy kpc² is among the smallest known. The detection of such pulsars is therefore not easy. Nevertheless, this may owe more to the state of our detection technology than to the intrinsic rarity of such “faint” neutron stars.

We have compiled information about all known young rotation-powered pulsars, defined here somewhat arbitrarily as those with $\tau_c < 30$ kyr (see the catalog of Manchester et al. 2005, but some of the distances used here are from original references). There are 36 such pulsars, of which 33 have been detected at radio wavelengths. Of these, 23 have a “high luminosity” L_{1400} (18–140 mJy kpc²; median 56 mJy kpc²): 14 have been long known (of which three were first detected as X-ray pulsars) and nine were discovered in the Parkes multibeam Galactic plane survey (e.g., Kramer et al. 2003b). With PSR J1833–1034, we know today of 10 young “low-luminosity” pulsars (0.5–6.3 mJy kpc²; median 2.4 mJy kpc²). Seven of these were detected in deep searches of PWNe (Halpern et al. 2001; Murray et al. 2002; Camilo et al. 2002a,b,c,d; Roberts et al. 2002, and this work), two more were detected in the Parkes multibeam survey (Camilo et al. 2001, 2004), and only one has been long known (B1853+01, discovered in a directed search of SNR W44; Wolszczan, Cordes, & Dewey 1991). Evidently, such pulsars are not so rare, but merely require more effort to uncover.

4. SUMMARY

We have discovered the 61.8 ms pulsar J1833–1034 at the center of the composite SNR G21.5–0.9 (§ 2.1). Second only to the Crab in spin-down luminosity among known rotation-powered Galactic pulsars, with $\dot{E} = 3.3 \times 10^{37}$ ergs s^{−1} (§ 2.2), PSR J1833–1034 was born in the SN explosion that gave rise to G21.5–0.9, which we estimate from the properties of the pulsar, PWN, and SNR shell occurred $\lesssim 1000$ years ago. This is substantially smaller than the pulsar characteristic age and in the simplest interpretation implies a birth spin period of \gtrsim

55 ms (§ 3.3), providing further evidence for a relatively large range in initial periods for neutron stars (e.g., Migliazzo et al. 2002; Kramer et al. 2003a).

PSR J1833–1034 is exceedingly weak at the radio frequency of 1.4 GHz used at the Parkes telescope to first detect it. We have revisited the distance to G21.5–0.9 based on HI and CO observations, and find the best estimate to be 4.7 ± 0.4 kpc (§ 3.1), for which the pulse-averaged luminosity at 1.4 GHz is about 1.5 mJy kpc², one of the smallest known for a young pulsar. Observations at other frequencies with the GBT (§ 2.2) suggest that J1833–1034 has an unusually steep spectrum, both of which findings have significant implications for the detection of additional very young pulsars and for studies of the radio luminosity, beaming fraction, and birth rate of such neutron stars (§ 3.5).

We have analyzed a large number of *Chandra* X-ray observations of the system and obtained the best image to date of the inner core of G21.5–0.9. This shows clear evidence for a pulsar component offset from the center of a surrounding very compact elliptical emission region that likely bounds the termination shock of the pulsar wind (§ 2.3). From this, under the assumption of energy equipartition in the PWN, we have obtained an estimate of the nebular magnetic field that is consistent with other determinations and plausibly is also broadly compatible with the X-ray and radio surface brightness and spectral energy distribution observed in the PWN (§ 3.2). PSR J1833–1034 has present-day spin parameters very similar to those of PSR J0205+6449 in SNR 3C 58, while the respective PWNe exhibit some significantly different properties (§ 3.4).

We have searched for X-ray pulsations from PSR J1833–1034 without success (§ 2.4). Our pulsed fraction limit for an assumed sinusoidal pulse shape is about 70% of the point-like luminosity of $3 \times 10^{-5}\dot{E}$. Depending on the rotational stability of the pulsar, to be determined from timing observations, we may in future obtain a better limit or, if the X-ray beam intersects our line of sight, a detection of such emission. Interestingly, no EGRET γ -ray source is known at the location of J1833–1034 (Hartman et al. 1999) — despite the fact that this neutron star has the fourth largest spin-down flux (\dot{E}/d^2) among known rotation-powered pulsars (after the Crab, Vela, and J0205+6449, which also is not a known γ -ray emitter; Camilo et al. 2002d). Assuming it beams toward the Earth, its efficiency for converting rotational power into > 100 MeV γ rays is relatively low, in keeping with a suggested inverse relation with \dot{E} (Thompson et al. 1999). Certainly, PSR J1833–1034 should be a prime target for the future *Gamma-ray Large Area Space Telescope*.

We thank Don Backer, David Kaplan, and Bryan Jacoby for their contributions to developing pulsar observing equipment at GBT, Jereon Stil for providing an absorption spectrum from the VLA Galactic Plane Survey, and Tom Dame for providing CO data and useful advice. We also acknowledge useful discussions with Jules Halpern, Roger Chevalier and Rino Bandiera. We are grateful to the dedicated staff at Parkes and GBT who make observing there such a productive pleasure. The Parkes Observatory is part of the Australia Telescope, which is funded by the Commonwealth of Australia for operation as a National Facility managed by CSIRO. The National Radio Astronomy Observatory is a facility of the National Science Foundation, operated under cooperative agreement by Associated Universities, Inc. We have made exten-

sive use of NASA's indispensable Astrophysics Data System. FC acknowledges support from NSF, NASA, and the NRAO travel fund. BMG and POS acknowledge support from NASA

through grants NAG5-13032 and NAG5-9281, and through contract NAS8-39073. DRL is a University Research Fellow funded by the Royal Society.

REFERENCES

- Altenhoff, W. J., Downes, D., Goad, L., Maxwell, A., & Rinehart, R. 1970, *A&AS*, 1, 319
- Backer, D. C., Dexter, M. R., Zepka, A., Ng, D., Wertheimer, D. J., Ray, P. S., & Foster, R. S. 1997, *PASP*, 109, 61
- Bandiera, R., Neri, R., & Cesaroni, R. 2001, in *AIP Conf. Proc. 565: Young Supernova Remnants*, ed. S. S. Holt & U. Hwang (New York: AIP), 329
- Becker, R. H., & Szymkowiak, A. E. 1981, *ApJ*, 248, L23
- Becker, W., & Trümper, J. 1997, *A&A*, 326, 682
- Belfort, P., & Crovisier, J. 1984, *A&A*, 136, 368
- Bietenholz, M. F., Kassim, N. E., & Weiler, K. W. 2001, *ApJ*, 560, 772
- Bietenholz, M. F., Kronberg, P. P., Hogg, D. E., & Wilson, A. S. 1991, *ApJ*, 373, L59
- Bird, A. J., et al. 2004, *ApJ*, 607, L33
- Blondin, J. M., Chevalier, R. A., & Frierson, D. M. 2001, *ApJ*, 563, 806
- Bocchino, F., van der Swaluw, E., Chevalier, R., & Bandiera, R. 2005, *A&A*, in press (astro-ph/0507518)
- Bocchino, F., Warwick, R. S., Marty, P., Lumb, D., Becker, W., & Pigot, C. 2001, *A&A*, 369, 1078
- Bock, D. C.-J., Wright, M. C. H., & Dickel, J. R. 2001, *ApJ*, 561, L203
- Camilo, F., Kaspi, V. M., Lyne, A. G., Manchester, R. N., Bell, J. F., D'Amico, N., McKay, N. P. F., & Crawford, F. 2000, *ApJ*, 541, 367
- Camilo, F., Lorimer, D. R., Bhat, N. D. R., Gotthelf, E. V., Halpern, J. P., Wang, Q. D., Lu, F. J., & Mirabal, N. 2002a, *ApJ*, 574, L71
- Camilo, F., Manchester, R. N., Gaensler, B. M., & Lorimer, D. R. 2002b, *ApJ*, 579, L25
- Camilo, F., Manchester, R. N., Gaensler, B. M., Lorimer, D. R., & Sarkissian, J. 2002c, *ApJ*, 567, L71
- Camilo, F., et al. 2001, *ApJ*, 557, L51
- Camilo, F., et al. 2002d, *ApJ*, 571, L41
- Camilo, F., et al. 2004, *ApJ*, 611, L25
- Caswell, J. L., Murray, J. D., Roger, R. S., Cole, D. J., & Cooke, D. J. 1975, *A&A*, 45, 239
- Chevalier, R. A. 2005, *ApJ*, 619, 839
- Cognard, I., Shrauner, J. A., Taylor, J. H., & Thorsett, S. E. 1996, *ApJ*, 457, 81
- Cordes, J. M., & Lazio, T. J. W. 2002, preprint (astro-ph/0207156)
- Crawford, F., Pivovarov, M. J., Kaspi, V. M., & Manchester, R. N. 2002, in *ASP Conf. Ser. 271: Neutron Stars in Supernova Remnants*, ed. P. O. Slane & B. M. Gaensler (San Francisco: ASP), 37
- Dame, T. M., Hartmann, D., & Thaddeus, P. 2001, *ApJ*, 547, 792
- Davelaar, J., Smith, A., & Becker, R. H. 1986, *ApJ*, 300, L59
- Dickel, J. R., & Wang, S. 2004, in *Young Neutron Stars and Their Environments*, IAU Symposium 218, ed. F. Camilo & B. M. Gaensler (San Francisco: ASP), 221
- Fesen, R. A., Martin, C. L., & Shull, J. M. 1992, *ApJ*, 399, 599
- Fich, M., Blitz, L., & Stark, A. A. 1989, *ApJ*, 342, 272
- Fürst, E., Handa, T., Morita, K., Reich, P., Reich, W., & Sofue, Y. 1988, *PASJ*, 40, 347
- Gaensler, B. M., van der Swaluw, E., Camilo, F., Kaspi, V. M., Baganoff, F. K., Yusef-Zadeh, F., & Manchester, R. N. 2004, *ApJ*, 616, 383
- Gallant, Y. A., & Tuffs, R. J. 1998, *Mem. Soc. Astron. Italiana*, 69, 963
- Green, D. A. 2004, *Bulletin of the Astronomical Society of India*, 32, 335
- Gregory, P. C., & Lored, T. J. 1992, *ApJ*, 398, 146
- Gupta, Y., Mitra, D., Green, D. A., & Acharyya, A. 2005, *Current Science*, submitted (astro-ph/0508257)
- Halpern, J. P., Camilo, F., Gotthelf, E. V., Helfand, D. J., Kramer, M., Lyne, A. G., Leighly, K. M., & Eracleous, M. 2001, *ApJ*, 552, L125
- Hartman, R. C., et al. 1999, *ApJS*, 123, 79
- Hartmann, D., & Burton, W. B. 1997, *Atlas of Galactic Neutral Hydrogen* (Cambridge: CUP)
- Haslam, C. G. T., Stoffel, H., Salter, C. J., & Wilson, W. E. 1982, *A&AS*, 47, 1
- Helfand, D. J., & Becker, R. H. 1987, *ApJ*, 314, 203
- Hessels, J. W. T., Roberts, M. S. E., Ransom, S. M., Kaspi, V. M., Romani, R. W., Ng, C.-Y., Freire, P. C. C., & Gaensler, B. M. 2004, *ApJ*, 612, 389
- Hobbs, G., Lorimer, D. R., Lyne, A. G., & Kramer, M. 2005, *MNRAS*, 360, 974
- Jackson, J. M., Bania, T. M., Simon, R., Kolpak, M., Clemens, D. P., & Heyer, M. 2002, *ApJ*, 566, L81
- Johnston, S., & Romani, R. W. 2003, *ApJ*, 590, L95
- Kaplan, D. L., et al. 2005, *PASP*, 117, 643
- Kaspi, V. M., Manchester, R. N., Johnston, S., Lyne, A. G., & D'Amico, N. 1996, *AJ*, 111, 2028
- Kaspi, V. M., Roberts, M. S. E., Vasisht, G., Gotthelf, E. V., Pivovarov, M., & Kawai, N. 2001, *ApJ*, 560, 371
- Kennel, C. F., & Coroniti, F. V. 1984, *ApJ*, 283, 694
- Koyama, K., Petre, R., Gotthelf, E. V., Hwang, U., Matura, M., Ozaki, M., & Holt, S. S. 1995, *Nature*, 378, 255
- Kramer, M., Lyne, A. G., Hobbs, G., Löhmer, O., Carr, P., Jordan, C., & Wolszczan, A. 2003a, *ApJ*, 593, L31
- Kramer, M., et al. 2003b, *MNRAS*, 342, 1299
- La Palombara, N., & Mereghetti, S. 2002, *A&A*, 383, 916
- Liszt, H. S., Burton, W. B., & Bania, T. M. 1981, *ApJ*, 246, 74
- Lorimer, D. R., & Kramer, M. 2005, *Handbook of Pulsar Astronomy* (Cambridge: CUP)
- Lorimer, D. R., Yates, J. A., Lyne, A. G., & Gould, D. M. 1995, *MNRAS*, 273, 411
- Lyne, A. G., & Lorimer, D. R. 1994, *Nature*, 369, 127
- Manchester, R. N., Hobbs, G. B., Teoh, A., & Hobbs, M. 2005, *AJ*, 129, 1993
- Manchester, R. N., & Taylor, J. H. 1977, *Pulsars* (San Francisco: Freeman)
- Manchester, R. N., et al. 2001, *MNRAS*, 328, 17
- Matheson, H., & Safi-Harb, S. 2005, *Advances in Space Research*, 35, 1099
- Migliazzo, J. M., Gaensler, B. M., Backer, D. C., Stappers, B. W., van der Swaluw, E., & Strom, R. G. 2002, *ApJ*, 567, L141
- Murray, S. S., Slane, P. O., Seward, F. D., Ransom, S. M., & Gaensler, B. M. 2002, *ApJ*, 568, 226
- Ng, C.-Y., & Romani, R. W. 2004, *ApJ*, 601, 479
- Pacholczyk, A. G. 1970, *Radio Astrophysics* (San Francisco: Freeman)
- Possenti, A., Cerutti, R., Colpi, M., & Mereghetti, S. 2002, *A&A*, 387, 993
- Ransom, S., Camilo, F., Kaspi, V., Slane, P., Gaensler, B., Gotthelf, E., & Murray, S. 2004, in *AIP Conf. Proc. 714: X-ray Timing 2003: Rossi and Beyond*, ed. P. Kaaret, F. K. Lamb, & J. H. Swank (New York: AIP), 350
- Ransom, S. M. 2001, PhD thesis, Harvard University
- Ransom, S. M., Eikenberry, S. S., & Middleditch, J. 2002a, *AJ*, 124, 1788
- Ransom, S. M., Gaensler, B. M., & Slane, P. O. 2002b, *ApJ*, 570, L75
- Ransom, S. M., Hessels, J. W. T., Stairs, I. H., Freire, P. C. C., Camilo, F., Kaspi, V. M., & Kaplan, D. L. 2005, *Science*, 307, 892
- Reynolds, S. P., & Chevalier, R. A. 1984, *ApJ*, 278, 630
- Roberts, M. S. E., Hessels, J. W. T., Ransom, S. M., Kaspi, V. M., Freire, P. C. C., Crawford, F., & Lorimer, D. R. 2002, *ApJ*, 577, L19
- Safi-Harb, S., Harrus, I. M., Petre, R., Pavlov, G. G., Koptsevich, A. B., & Sanwal, D. 2001, *ApJ*, 561, 308
- Salter, C. J., Reynolds, S. P., Hogg, D. E., Payne, J. M., & Rhodes, P. J. 1989, *ApJ*, 338, 171
- Seward, F. D., & Wang, Z.-R. 1988, *ApJ*, 332, 199
- Shaver, P. A., Radhakrishnan, V., Anantharamaiah, K. R., Retallack, D. S., Wamsteker, W., & Danks, A. C. 1982, *A&A*, 106, 105
- Slane, P., Chen, Y., Schulz, N. S., Seward, F. D., Hughes, J. P., & Gaensler, B. M. 2000, *ApJ*, 533, L29
- Slane, P., Gaensler, B. M., Dame, T. M., Hughes, J. P., Plucinsky, P. P., & Green, A. 1999, *ApJ*, 525, 357
- Slane, P., Helfand, D. H., van der Swaluw, E., & Murray, S. S. 2004, *ApJ*, 616, 403
- Staveley-Smith, L., et al. 1996, *Proc. Astr. Soc. Aust.*, 13, 243
- Stephenson, F. R., & Green, D. A. 2002, *Historical Supernovae and their Remnants* (Oxford: OUP)
- Taylor, A. R., Stil, J. M., Dickey, J. M., McClure-Griffiths, N. M., Martin, P. G., Rothwell, T., & Lockman, F. J. 2002, in *ASP Conf. Ser. 276: Seeing Through the Dust: The Detection of HI and the Exploration of the ISM in Galaxies*, ed. A. R. Taylor, T. L. Landecker, & A. G. Willis (San Francisco: ASP), 68
- Thompson, D. J., et al. 1999, *ApJ*, 516, 297
- van der Swaluw, E. 2003, *A&A*, 404, 939
- van der Swaluw, E., Achterberg, A., Gallant, Y. A., & Tóth, G. 2001, *A&A*, 380, 309
- Warwick, R. S., et al. 2001, *A&A*, 365, L248
- Wilson, A. S., & Weiler, K. W. 1976, *A&A*, 53, 89
- Wilson, T. L., & Altenhoff, W. 1970, *Astrophys. Lett.*, 5, 47
- Wolszczan, A., Cordes, J. M., & Dewey, R. J. 1991, *ApJ*, 372, L99

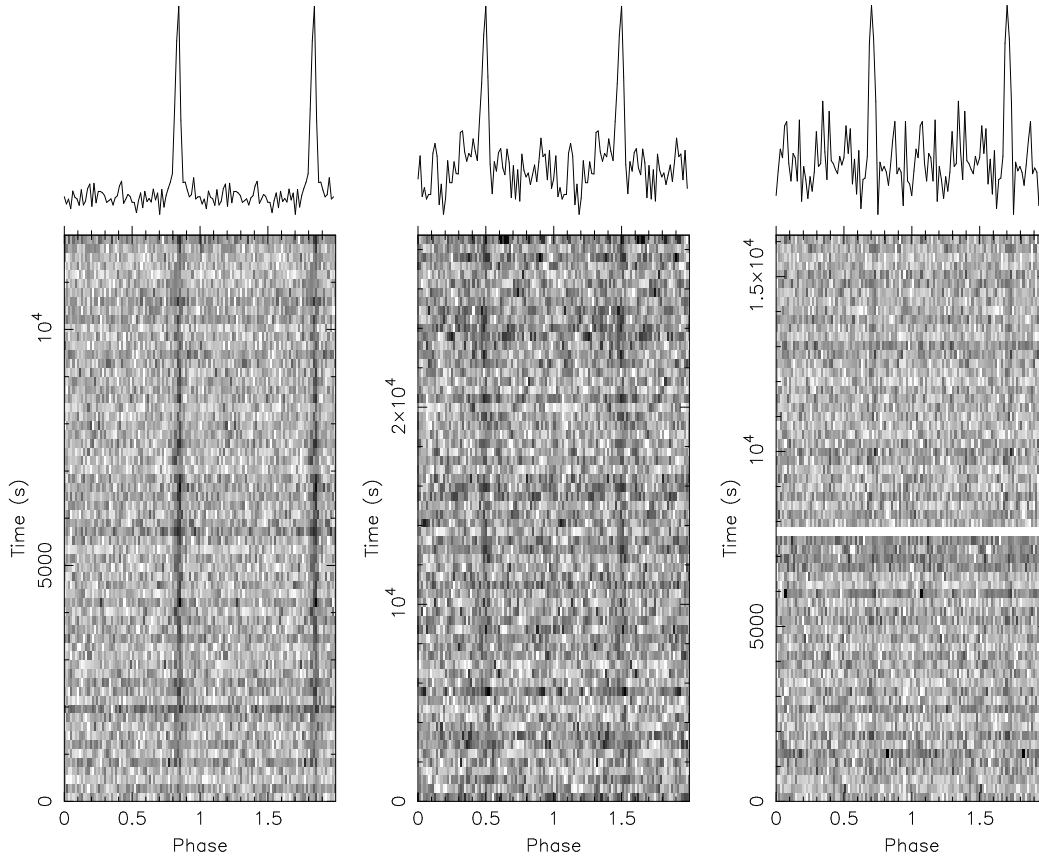


FIG. 1.— Radio pulse profiles of PSR J1833–1034. Central frequencies increase from left to right: 820 MHz (GBT), 1374 MHz (Parkes; discovery observation), and 1850 MHz (GBT). In each plot, the linear grey-scale represents pulsar strength as a function of rotational phase and time (increasing from bottom), with the total observation split into and displayed as 64 sub-integrations. At top is shown the summed pulse profile for the full observation. Two pulse periods are shown in all cases. The 1850 MHz profile was obtained from a bandwidth of 400 MHz (the pulsar was not detected in the upper 200 MHz of bandwidth recorded with SPIGOT; see Table 1), and the white band indicates removal of data due to interference. There is evidence of apparent interstellar scintillation in the time-varying flux densities of the 820 MHz and possibly 1374 MHz data sets (and the nominal flux densities for separate 820 MHz and 1374 MHz observations differ by $\sim 10\%$ – 30% ; see Table 1). The observed pulse full-width at half-maximum is 3.0 ms ($0.05P$) at 1374 MHz and 2.5 ms at the other two frequencies. Smearing due to differential dispersive propagation within one frequency channel is 1.3 ms for the 820 MHz data and 1.6 ms for the 1374 MHz data (which, additionally, have a sample interval of 0.8 ms). Therefore, the intrinsic pulse FWHM is very nearly $0.04P$ at all frequencies.

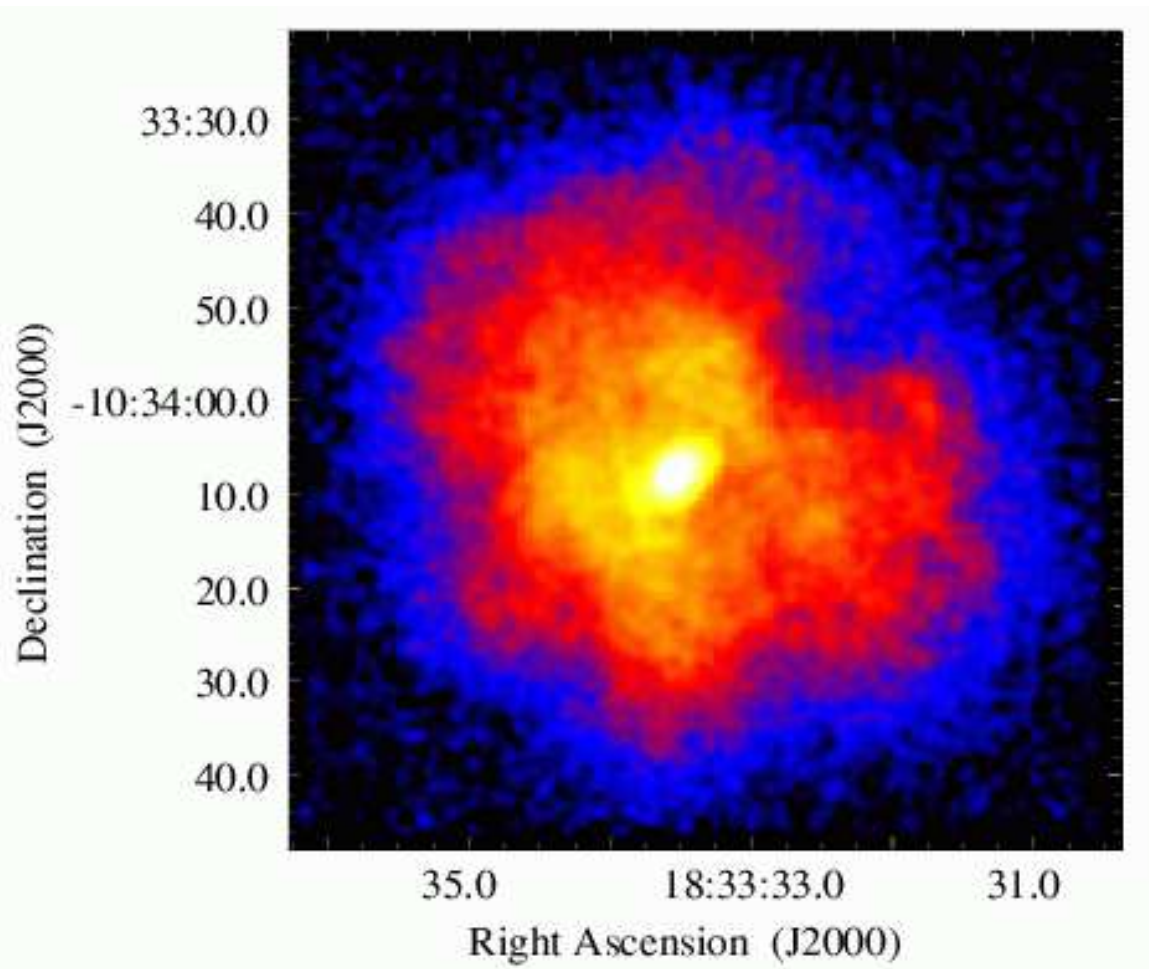


FIG. 2.— False-color *Chandra* ACIS-S image of the PWN in SNR G21.5–0.9 based on 58 ks of data, showing the elongated core embedded in the more diffuse nebula. The SNR shell lies beyond the edge of this image. The image has been smoothed by two pixels ($0''.98$), and the intensity levels increase logarithmically from a surface brightness of $9 \text{ cts arcsec}^{-2}$ in the outer regions (blue) to a value of $1640 \text{ cts arcsec}^{-2}$ in the core (white). See § 2.3 for further details about the image.

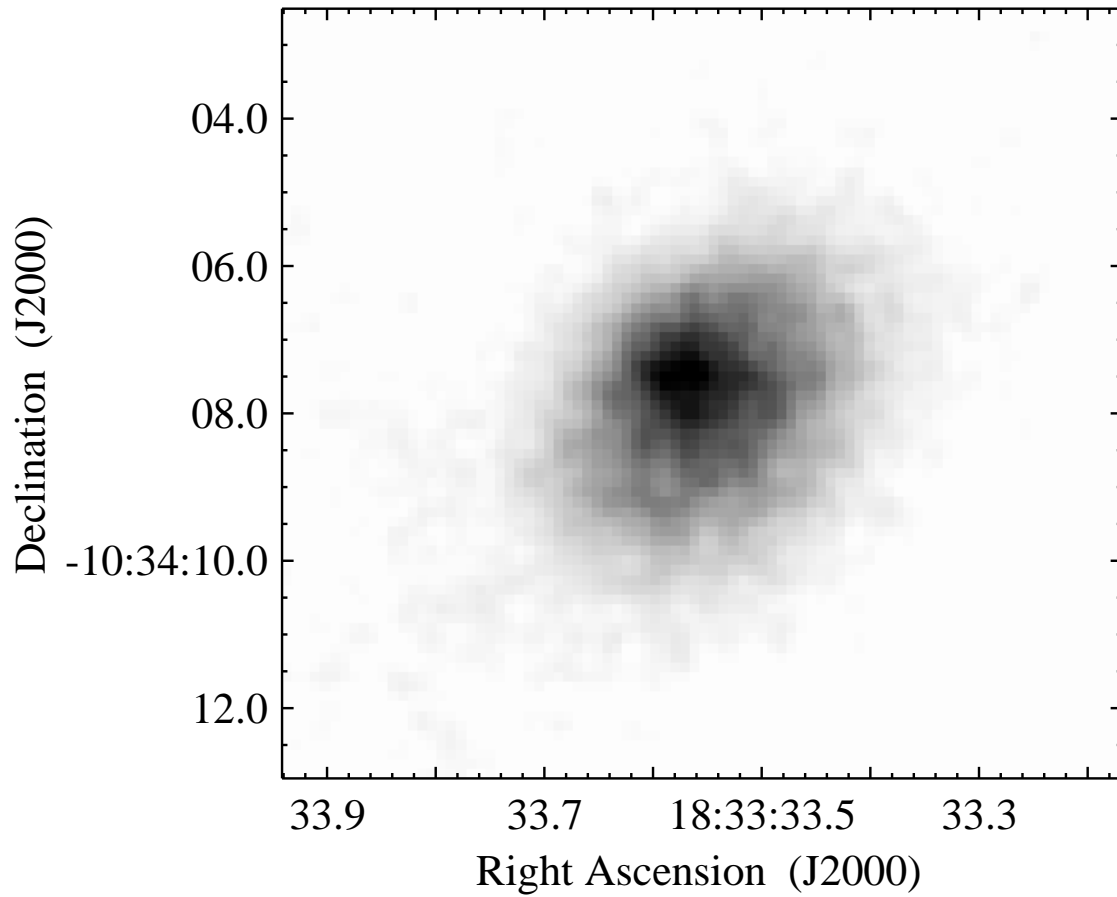


FIG. 3.— Grey-scale *Chandra* HRC image of the central core in G21.5–0.9 based on 351 ks of data from multiple observations (compare to Fig. 2). The image has been smoothed by two pixels ($0''.26$), and any residual registration error/blurring is at the level of $< 0''.3$. A compact source, presumably corresponding to PSR J1833–1034, is surrounded by an elongated emission region. The grey-scale intensity increases linearly from $520 \text{ cts arcsec}^{-2}$ at the outer edge of the core (e.g., near R.A. $18^{\text{h}}33^{\text{m}}33^{\text{s}}.5$, Decl. $-10^{\circ}34'05''.5$) to $2500 \text{ cts arcsec}^{-2}$ at the position of the compact source. See §§ 2.3 and 2.4 for more details.